J. Phys. B: At. Mol. Opt. Phys. **41** (2008) 125401 (8pp) doi:10.1088/0953-4075/41/12/125401

Double radio-optical resonance in ^{87}RB atomic vapour in a finite-size bufferless cell

Andrey Litvinov[1], Georgy Kazakov[2], Boris Matisov[2] and Igor Mazets[3]

[1] Solid State Physics Department, A. F. Ioffe Physico-Technical Institute, Polytechnicheskaya 26, St Petersburg, 194021, Russia
[2] Theoretical Physics Department, St Petersburg State Polytechnical University, Polytechnicheskaya 29, St Petersburg, 195251, Russia
[3] Plasma Physics Department, A. F. Ioffe Physico-Technical Institute, Polytechnicheskaya 26, St Petersburg, 194021, Russia

E-mail: anprolvy@list.ru, kazjor@rambler.ru and mazets@astro.ioffe.rssi.ru

Received 3 February 2008, in final form 13 May 2008
Published 9 June 2008
Online at stacks.iop.org/JPhysB/41/125401

Abstract
We study theoretically the formation of a double radio-optical resonance (DROR) in ^{87}Rb vapour in a cell with an anti-relaxation coating. We develop a quantum-kinetic approach to the study of the Dicke narrowing. We examine various DROR schemes for different polarizations of the laser radiation. We find that the short-term stability σ_y of a DROR-based frequency standard improves significantly (by an order of magnitude) if a laser with a broad spectrum is used, in comparison to the case of excitation by a narrow-band laser radiation, and reaches ultimately the value $\sigma_y \sim 1 \times 10^{-14}\,\tau^{-1/2}$, where τ is the integration time (in seconds).

1. Introduction

Resonant interaction of two electromagnetic waves (optical and radiofrequency) with atoms is known as the double radio-optical resonance (DROR). This effect has been used for the creation of magnetometers [1–4] and quantum frequency standards [4, 5]. Unprecedented precision of the most up-to-date techniques of magnetic field measurement [6, 7] makes optical magnetometers very promising tools for various branches of both fundamental and applied science, such as detecting weak magnetic fields of human heart and brain [8] or space research [9]. Moreover nonlinear optics of four-level (and, in general, multilevel) quantum systems irradiated by combined optical and microwave fields is now of wide interest. For example, sharp and high-contrast resonances in Rb irradiated by resonant coherent optical and microwave fields, theoretically studied in [10], were observed in [11].

No less significant are the fields of the application of quantum frequency standards, including building up global systems of navigation and positioning, synchronization services in telecommunication networks and experimental tests of the fundamental laws of physics.

A quantum discriminator is the principal part of a quantum frequency standard. Its performance is characterized by the figure of merit Q, which is determined by the amplitude and the width of the resonance used for locking and stabilizing the frequency. These parameters depend on the time of coherent interaction of the atoms with the resonant electromagnetic fields. The main factor that destroys the atom–field coherence is the depolarization (angular-momentum randomization) of an atom during its collision with a cell wall. Another adverse factor is the thermal motion of an atom: the phase of the electromagnetic field acting to atom changes in time, as the atom traverses the distance comparable to the wavelength λ of the microwave radiation. Therefore, to improve the figure of merit, one has to extend the time of the coherent atom–field interaction.

There are two main methods to increase this time: adding a buffer gas into the cell containing the active atoms and covering the cell walls with an anti-relaxant material. The depolarization of active atoms caused by their collisions with the atoms (or molecules) of the buffer gas is practically negligible. However, the mean free path of active atoms becomes significantly shorter. As a result, the frequency of collision of the active atoms with the cell walls and, hence, the

corresponding depolarization rate are reduced. In contrast, the time required for an atom to travel to the distance of the order of λ in the diffusion regime grows. This method has several disadvantages, the most serious one being the shift and the broadening of the frequency of the working (etalon) transition due to exchange (Pauli) repulsion and van der Waals attraction between the paramagnetic active atoms and the diamagnetic atoms or molecules of the buffer gas.

The second method (anti-relaxation covering of the cell walls), known for a long time [12], is free of these disadvantages. The depolarization probability per collision of an active atom with a cell wall coated by an anti-relaxant (most commonly, paraffin is used for this purpose) drops by four orders of magnitude [13], compared to the case of an uncoated cell. Previous objections against anti-relaxation coatings, because of their allegedly rapid ageing, have been refuted recently [1]: the shift of the microwave transition frequency has been proven to be less than 10 Hz in 30 years. This makes DROR in coated cells a very promising line of research, since the resonance width in such cells may be as narrow as 47 Hz [14].

In the present work, we analyse DROR in ^{87}Rb vapour in a cell without a buffer gas. We numerically solve the set of quantum kinetic equations for the atomic density matrix, the presence or absence of the wall coating being taken into account via boundary conditions. In contrast to [15], where the DROR is analysed within the idealized three-level model and the DROR excitation is provided by an incoherent radiation source (a gas discharge lamp), in the present work we take into account the full hyperfine and Zeeman structure of the ground and excited states of ^{87}Rb and consider the DROR excitation by the laser (coherent) radiation. Special attention is paid to the theoretical study of the dependence of the DROR parameters on the width of the laser radiation spectrum. We find that the excitation of atomic systems by a coherent (laser) radiation can result in new effects.

2. The set of quantum kinetic equations

Consider a ^{87}Rb atom that interacts with two electromagnetic fields, laser and microwave. The constant external magnetic field **B** lifts the degeneracy of the atomic levels with respect to the projection of the total angular momentum to the quantization axis defined by the magnetic field direction. We denote the levels of the ground ($S_{1/2}$) and excited ($P_{1/2}$ or $P_{3/2}$) states of the ^{87}Rb atom by g and e, respectively. We further divide the ground-state sublevels into two subgroups, g_1 and g_2, with regard to the corresponding value of the total angular momentum $F_g = 1$ and $F_g = 2$ (see figure 1).

The electric component **E** of the optical field and the magnetic component **H** of the microwave field are the running waves:

$$\mathbf{E}(\mathbf{r}, t) = \mathbf{E}_0 \exp\left[\mathrm{i}\left(\mathbf{kr} - \omega t\right)\right] + \text{c.c.}, \tag{1}$$

$$\mathbf{H}(\mathbf{r}, t) = \mathbf{H}_0 \exp\left[\mathrm{i}\left(\mathbf{qr} - \omega_{\mathrm{rf}} t\right)\right] + \text{c.c.}, \tag{2}$$

with $\mathbf{E}_0$ and $\mathbf{H}_0$ being their amplitudes, **k** and **q** being their wave vectors, ω and ω_{rf} being their frequencies. The optical field

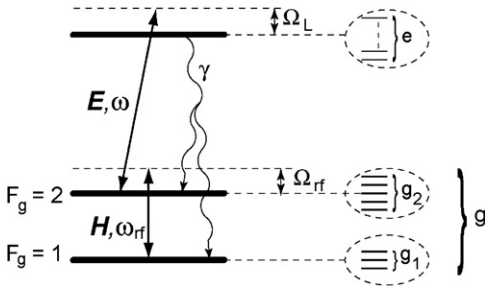

Figure 1. General sketch of the DROR excitation scheme (see the text for details).

drives the electric dipole transition $|F_g = 2\rangle \leftrightarrow |F_e\rangle$ between the ground and the first excited state; the microwave field drives the magnetic dipole transition $|F_g = 1\rangle \leftrightarrow |F_g = 2\rangle$ between hyperfine sublevels of the ground state. The atomic density matrix $\widehat{\rho}(\mathbf{r}, \mathbf{p}, t)$ in the Wigner representation evolves according to the equation

$$\dot{\rho}_{ij}(\mathbf{r}, \mathbf{p}, \mathbf{t}) \equiv \frac{\partial \rho_{ij}}{\partial t} + \frac{\mathbf{p}}{m}\nabla\rho_{ij}$$

$$= -\frac{\mathrm{i}}{\hbar}\sum_k \left[H_{ik}\rho_{kj} - \rho_{ik}H_{kj}\right] + (\widehat{\widehat{\Gamma}}\,\widehat{\rho})_{ij}. \tag{3}$$

Here H_{ij} is the matrix element of the Hamiltonian $\widehat{H}$, the subscripts i and j denote the atomic states, $\widehat{\widehat{\Gamma}}$ is the relaxation operator and m is the atomic mass. The Hamiltonian $\widehat{H}$ can be represented as

$$\widehat{H} = \widehat{H}_0 + \hbar\widehat{V}, \tag{4}$$

where $\widehat{H}_0$ is the atomic Hamiltonian in the absence of the external radiation and $\hbar\widehat{V}$ describes the interaction of the atom with the optical and microwave fields:

$$\widehat{V} = \sum_{e,g_2} |e\rangle V^0_{\mathrm{eg_2}} \exp[\mathrm{i}(\mathbf{kr} - \omega t)]\langle \mathrm{g_2}| + \sum_{g_2 g_1} |\mathrm{g_2}\rangle U^0_{\mathrm{g_1 g_2}}$$
$$\times \exp\left[\mathrm{i}(\mathbf{qr} - \omega_{\mathrm{rf}} t)\right] \langle \mathrm{g_1}| + \text{h.c.}, \tag{5}$$

where $V^0_{\mathrm{eg_2}}$ and $U^0_{\mathrm{g_1 g_2}}$ are the Rabi frequencies for the optically- and microwave-driven transitions, respectively.

Consider then the matrix elements $\Gamma_{ij,kl}$ of the relaxation operator $\widehat{\widehat{\Gamma}}$ in equation (3). The elements $\Gamma_{\mathrm{ee,ee}} = -\gamma \approx -3.5 \times 10^7\ c^{-1}$ define the rate of the decay of the excited state due to spontaneous relaxation. The return of the atomic population to the ground state is described by the matrix elements $\Gamma_{\mathrm{gg,ee}} = \gamma P_{\mathrm{ge}}$, where P_{ge} is the probability for an atom to occur in the state g after spontaneous decay of the state e (the branching ratio) [16]:

$$P_{\mathrm{ge}} = (2F_g + 1)(2J_e + 1) \cdot \left(C^{F_e m_e}_{F_g m_g 1 R} \begin{Bmatrix} J_g & I & F_g \\ F_e & 1 & J_e \end{Bmatrix} \right)^2. \tag{6}$$

Here J_e and J_g are the electronic angular momenta, F_e and F_g the total momenta, arising from coupling J_e (or, respectively, J_g) to the nuclear spin I ($I = 3/2$ for ^{87}Rb), m_e and m_g are the projections of the total momenta to the quantization axis, the subscript g or e indicates the values for

the ground or the excited state, respectively, $R = m_e - m_g$, $C^{F_e m_e}_{F_g m_g 1 R}$ is the Clebsch–Gordan coefficient, and $\{\cdots\}$ is the 6J symbol.

In the absence of a buffer gas, the decay of the off-diagonal density matrix elements ρ_{eg} (the so-called optical coherences) is given by $\Gamma_{eg,eg} = -\gamma'$ with $\gamma' = \gamma/2$ [17]. The relaxation of the 'microwave coherences' $\rho_{gg'}$, $g \neq g'$ is given by $\Gamma_{gg',gg'} = -\Gamma_\perp$. It is caused by collisions of the active atoms to each other and thus is proportional to their number density, which, in turn, is determined by the cell temperature. The depolarization processes in the ground state manifold are described by the matrix elements $\Gamma_{gg,g'g'} = \Gamma_\parallel \tilde{P}_{gg'}$, $g \neq g'$ and $\Gamma_{gg,gg} = -\Gamma_\parallel$, where $\Gamma_\parallel \leqslant \Gamma_\perp$ is the depolarization rate and $\tilde{P}_{gg'}$ is the normalized to 1 probability for an atom to change its internal state from g′ to g in the course of an inelastic (spin-changing) collision. Without loss of generality, we assume that all these transitions are equally probable $\left(\tilde{P}_{gg'} = \left(2\left(F_{g_1} + F_{g_2}\right) + 1\right)^{-1},\ g \neq g'\right)$.

We assume that the optical field is tuned exactly in resonance with the respective transitions. Upon adiabatic elimination of ρ_{ee} and ρ_{eg}, we obtain the following set of equations (in the interaction representation) for the populations ρ_{gg} and coherences $\rho_{gg'}$ in the ground-state manifold:

$$\dot{\rho}_{g_1 g_1'} = -\mathrm{i}\left[\left(\omega_{g_1 g_1'} - \mathrm{i}\Gamma_\perp\right)\rho_{g_1 g_1'} + \sum_{g_2}\left(U^0_{g_1 g_2}\rho_{g_2 g_1'} - \rho_{g_1 g_2}U^0_{g_2 g_1'}\right)\right]$$
$$+ \delta_{g_1 g_1'}\left[\Gamma_\perp\rho_{g_1 g_1'} - \Gamma_\parallel\cdot\left(\rho_{g_1 g_1} - \sum_{g''}\tilde{P}_{g_1 g''}\rho_{g'' g''}\right)\right.$$
$$\left. + \sum_{e,g_2'',g_2'''} 2P_{g_1 e}\frac{V^0_{eg_1''}V^0_{g_1''' e}}{\gamma'}\tilde{G}_e\rho_{g_2'' g_2'''}\right],$$

$$\dot{\rho}_{g_2 g_2'} = -\mathrm{i}\left[\left(\omega_{g_2 g_2'} - \mathrm{i}\Gamma_\perp\right)\rho_{g_2 g_2'} + \sum_{g_1}\left(U^0_{g_2 g_1}\rho_{g_1 g_2'} - \rho_{g_2 g_1}U^0_{g_1 g_2'}\right)\right.$$
$$+ \sum_{e,g_2''}\frac{V^0_{g_2 e}V^0_{eg_2''}}{\gamma'}\left[\tilde{F}_e - \mathrm{i}\tilde{G}_e\right]\rho_{g_2'' g_2'}$$
$$\left. - \sum_{e,g_2''}\frac{V^0_{g_2'' e}V^0_{eg_2'}}{\gamma'}\left[\tilde{F}_e + \mathrm{i}\tilde{G}_e\right]\rho_{g_2 g_2''}\right]$$
$$+ \delta_{g_2 g_2'}\left[\Gamma_\perp\rho_{g_2 g_2'} - \Gamma_\parallel\cdot\left(\rho_{g_2 g_2} - \sum_{g''}\tilde{P}_{g_2 g''}\rho_{g'' g''}\right)\right.$$
$$\left. + \sum_{e,g_2'',g_2'''} 2P_{g_2 e}\frac{V^0_{eg_2''}V^0_{g_2''' e}}{\gamma'}\tilde{G}_e\right],$$

$$\dot{\rho}_{g_1 g_2} = -\mathrm{i}\left[(\omega_{rf} - \Delta_{se} - \omega_{g_2 g_1} - \mathbf{q}\cdot\upsilon - \mathrm{i}\Gamma_\perp)\rho_{g_1 g_2}\right.$$
$$+ \sum_{g_2'}U^0_{g_1 g_2'}\rho_{g_2' g_2} - \sum_{g_1'}\rho_{g_1 g_1'}U^0_{g_1' g_2}$$
$$\left. - \sum_{e,g_2'}\frac{V^0_{g_2' e}V^0_{eg_2}}{\gamma'}\left[\tilde{F}_e + \mathrm{i}\tilde{G}_e\right]\rho_{g_1 g_2'}\right]. \quad (7)$$

Here ω_{ij} is the frequency interval between the states i and j, $\upsilon = \mathbf{p}/m$ is the atomic velocity, δ_{ij} is the Kronecker symbol and Δ_{se} is the frequency shift caused by the spin-exchange interactions of atoms. The real coefficients $\tilde{F}_e$ and $\tilde{G}_e$ are defined as

$$\tilde{G}_e + \mathrm{i}\tilde{F}_e = \int_{-\infty}^{+\infty}\frac{\gamma'\cdot J(\omega')}{\gamma' - \mathrm{i}(\omega' - \omega_{eg_2} + \Omega_L - \mathbf{k}\upsilon)}\,\mathrm{d}\omega', \quad (8)$$

where $J(\omega')$ is the spectral density of the laser radiation, normalized to unity $\left(\int_{-\infty}^{+\infty}J(\omega')\,\mathrm{d}\omega' = 1\right)$. Since we consider the stationary regime, the time derivatives in equation (7) are set to zero.

Zeeman splitting of the magnetic sublevels of the hyperfine states g_1 and g_2 is about 0.7 MHz G^{-1}. In weak magnetic fields (<1 G) used in quantum discriminators for lifting the degeneracy this yields splitting values much less than the Doppler broadening $\Delta_D = 2\sqrt{\ln 2}\cdot k\upsilon_T$ of the optical transition (υ_T being the most probable velocity of the atoms at the temperature T) and the rate γ' of the optical coherence decay. Therefore, we neglect in equation (8) the dependence of ω_{eg_2} on the angular momentum projection.

The diffusion model of the laser radiation phase noise predicts the Lorentzian shape of the spectral intensity [18]:

$$J(\omega') = \frac{\Gamma_L/2\pi}{(\omega - \omega')^2 + \Gamma_L^2/4}, \quad (9)$$

with Γ_L being its width (FWHM). Then (8) reduces to

$$\tilde{G}_e + \mathrm{i}\tilde{F}_e = \frac{\gamma' + \Gamma_L/2}{\gamma' + \Gamma_L/2 - \mathrm{i}(\omega + \Omega_L - \mathbf{k}\upsilon)}. \quad (10)$$

If other types of noise dominate over the phase noise, the general formula (8) should be used.

The excited-state populations are

$$\rho_{exc} = \sum_{e,g_2'',g_2'''} 2\frac{V^0_{eg_2''}V^0_{g_2''' e}}{\gamma\gamma'}\tilde{G}_e\rho_{g_2'' g_2'''}. \quad (11)$$

Since at $T = 323$ K the Doppler width $\delta_D = 2\sqrt{\ln 2}\cdot q\upsilon_T$ of the microwave transition $|F_g = 1,\ m\rangle \leftrightarrow |F_g = 2,\ m\rangle$ is of about 8 kHz, and the difference between the frequencies of the working transition $|F_g = 1,\ m = 0\rangle \leftrightarrow |F_g = 2,\ m = 0\rangle$ and another hyperfine transition $|F_g = 1,\ m = \pm 1\rangle \leftrightarrow |F_g = 2,\ m = \pm 1\rangle$ is much larger (70 kHz for the external magnetic field B as small as 0.05 G), the microwave-induced transitions between the states $|F_g = 1,\ m = \pm 1\rangle$ and $|F_g = 2,\ m = \pm 1\rangle$ are off-resonant and can be neglected. It is convenient to introduce the microwave-field detuning

$$\Omega_{rf} = \omega_{rf} - \omega_{21}, \quad (12)$$

where $|1\rangle = |F_g = 1,\ m = 0\rangle$, $|2\rangle = |F_g = 2,\ m = 0\rangle$.

Since typical atomic velocity is much larger than the photon recoil velocity, and the number density of active atoms is low (their mean free path in a cell without a buffer gas is by several orders of magnitude longer than the cell size), we can treat the evolution of the density matrix as local with respect to both the coordinate and momentum. Thermal equilibrium for the atomic translational degrees of freedom results in the following normalization condition:

$$\sum_i \rho_{ii}(\mathbf{r},\mathbf{p},t) = \frac{M(p)}{V_{cell}}, \quad M(\mathbf{p}) = \frac{\exp\left(-\mathbf{p}^2/p_T^2\right)}{\left(p_T\sqrt{\pi}\right)^3}, \quad (13)$$

where $p_T = \sqrt{2k_B mT}$, k_B is Boltzmann's constant and V_{cell} is the cell volume.

In our model, we make the following assumptions regarding the collision of an active atom with the cell wall. Firstly, the kinetic momenta of an atom $\mathbf{p}$ and $\mathbf{p}'$ before and after the collision are related to each other as $\mathbf{p}' = \mathbf{p} - 2\mathbf{n}\cdot(\mathbf{n}\cdot\mathbf{p})$, where $\mathbf{n}$ is the unit vector normal to the inner surface S of the cell (mirror-like reflection). Secondly, the depolarization processes do not depend on $\mathbf{p}$. Finally, in a wall collision followed by depolarization, the transitions between different sublevels of the ground state occur with the same probability. Then the boundary conditions for the atomic density matrix can be written as

$$\bar{\rho}_{gg}(\mathbf{p}') - \rho_{gg}(\mathbf{r}, \mathbf{p}')_{\mathbf{r}\in S} = \beta(\bar{\rho}_{gg}(\mathbf{p}) - \rho_{gg}(\mathbf{r}, \mathbf{p})_{\mathbf{r}\in S}),$$
$$\rho_{gg'}(\mathbf{r}, \mathbf{p}')_{\mathbf{r}\in S} = \alpha \cdot \rho_{gg'}(\mathbf{r}, \mathbf{p})_{\mathbf{r}\in S}, \quad g \neq g'. \tag{14}$$

Here $\bar{\rho}_{gg}(\mathbf{p}) = M(\mathbf{p})/(8 \cdot V_{\text{cell}})$ is the diagonal element of the density matrix of completely depolarized atoms. The coefficients α and β ($0 \leqslant \alpha, \beta \leqslant 1$) characterize the degree of relaxation of atomic populations ρ_{gg} and coherences $\rho_{gg'}$ after a collision with the cell wall.

If the cell is coated with a special anti-relaxation material (e.g., long-chain paraffin), then atoms do not adsorb at the cell wall, and the collision-induced phase dispersion is also very small. Hence, significant depolarization requires a very high number of wall collisions. The idealized limiting case of this situation is represented by the boundary conditions of the specular-coherent type [15], implying that

$$\alpha = \beta = 1. \tag{15}$$

In the opposite limiting case each collision fully randomizes the atomic spin. Such a situation is typical for alkali metal vapours in uncoated glass cells. The reason is a high dispersion of local magnetic fields. For example, in a Pyrex glass, where the abundance of magnetite, which forms ferromagnetic domains, reaches 0.1%, the rms of the random local magnetic field is of about 5 G. This is sufficient to provide complete relaxation of coherences and equilibration of populations in atoms just after the collision with the wall. This corresponds to the complete quenching boundary conditions [15]:

$$\alpha = \beta = 0. \tag{16}$$

Solving numerically the set of equation (7) with the boundary conditions (14), using equation (8) and integrating over the cell volume and the kinetic momentum of an atom, we find the total population of atoms in the optically excited state:

$$\bar{\rho}_{\text{exc}} = \int\int \rho_{\text{exc}}(\mathbf{r}, \mathbf{p})\, d\mathbf{r}\, d\mathbf{p}. \tag{17}$$

The power δP of the laser radiation absorbed in the cell is proportional to $\bar{\rho}_{\text{exc}}$ [19]:

$$\delta P = \hbar\omega \cdot \gamma \cdot N \cdot \bar{\rho}_{\text{exc}}, \tag{18}$$

with N being the number of active atoms in the cell.

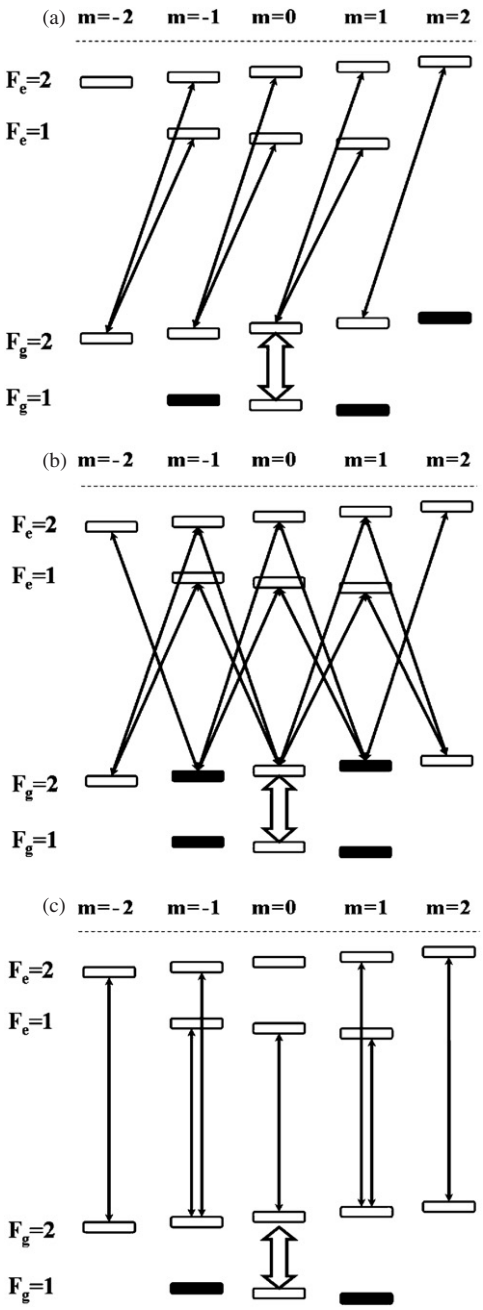

Figure 2. Excited transitions in the ^{87}Rb atom. The microwave field drives the working transition $|F_g = 1,\ m = 0\rangle \leftrightarrow |F_g = 2,\ m = 0\rangle$ (double arrow), the laser light drives the transitions $|F_g = 2\rangle \leftrightarrow |F_e\rangle$ (thin lines). The laser field polarization: (a) σ^+; (b) linear; (c) π.

3. The results of numerical calculations

In figure 2, we present different schemes of DROR, depending on the polarization of the laser radiation. In figure 2(a), the scheme of optical pumping by a σ^+-polarized light is shown. There are three idle levels ('pockets', denoted by black rectangles) $|F_g = 1,\ m = -1\rangle$, $|F_g = 2,\ m = +2\rangle$ and $|F_g = 1,\ m = 1\rangle$, which do not interact with the laser radiation. After few optical pumping cycles all the atoms accumulate in these 'pockets' and cease to contribute into the DROR signal formation. This significantly decreases

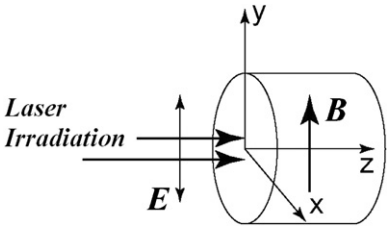

Figure 3. Geometrical configuration for the scheme of excitation by a π-polarized laser radiation.

the amplitude of the resonance and, hence, worsens the figure of merit. The $|F_g = 2,\ m = +2\rangle$ 'pocket' can be avoided by using linearly polarized light (figure 2(b)). However, a more detailed analysis shows that in the system of levels $|F_g = 2,\ m = -1\rangle$, $|F_g = 2,\ m = +1\rangle$ and $|F_e,\ m = 0\rangle$, coherently coupled by the laser field, the effect of coherent population trapping (CPT) arises [20]. In this situation, the influence of the CPT is negative: the atoms being accumulated in a coherent superposition of the levels $|F_g = 2,\ m = 1\rangle$ and $|F_g = 2,\ m = -1\rangle$ stop to contribute to the DROR signal formation [17].

Finally, consider the excitation scheme presented in figure 2(c) (π-polarization). This type of excitation is the most efficient, since the number of 'pockets' there is minimized. These 'pockets', associated with the states $|F_g = 1,\ m = -1\rangle$, $|F_g = 1,\ m = +1\rangle$, are also present in the two previous schemes. To avoid them, one has to apply two lasers for pumping [21, 22]. However, practical implementation of the latter scheme with two exactly perpendicular laser beams is challenging. Therefore, we consider in the present paper the single-laser optical pumping, which is used in most of the experiments.

From now on we consider the optimum scheme of figure 2(c) with the pumping by π-polarized laser radiation resonant to the D_1-line of ^{87}Rb (π-polarization corresponds to the light linearly polarized along the constant external magnetic field **B**, whereas the propagation direction of the light is perpendicular to **B**; for the sketch of the geometry of this scheme see figure 3).

The DROR signal is the dependence of the photodetector current j on the microwave field detuning Ω_{rf}. Since the absorbed radiation power and, hence, the variation of j are proportional to the excited-state population $\bar{\rho}_{exc}$, we call the DROR signal the dependence $\bar{\rho}_{exc}(\Omega_{rf})$. The definitions of the basic parameter of the resonance are the following [23]. The DROR amplitude is the difference $\bar{\rho}^{NR}_{exc} - \bar{\rho}^{R}_{exc}$ between the excited-state population far outside the resonance $\left(\bar{\rho}^{NR}_{exc}\right)$ and exactly in resonance $\left(\bar{\rho}^{R}_{exc}\right)$. The DROR width Γ_{DROR} is its FWHM. The contrast is defined as $C(\Omega_{rf}) = \frac{\bar{\rho}_{exc}(\Omega_{rf}) - \bar{\rho}^{NR}_{exc}}{\bar{\rho}_{exc}(\Omega_{rf})}$.

The optical field is tuned exactly in resonance with the transition $|F_g = 2\rangle \leftrightarrow |F_e = 1\rangle$. Since the hyperfine splitting of the excited state is 817 MHz and the Doppler width of the optical transition is $\Delta_D \approx 500$ MΓ_u, we also take into account optically-induced transitions $|F_g = 2\rangle \leftrightarrow |F_e = 2\rangle$. The working transition driven by the microwave radiation is $|F_g = 1,\ m = 0\rangle \leftrightarrow |F_g = 2,\ m = 0\rangle$, as usual, since only

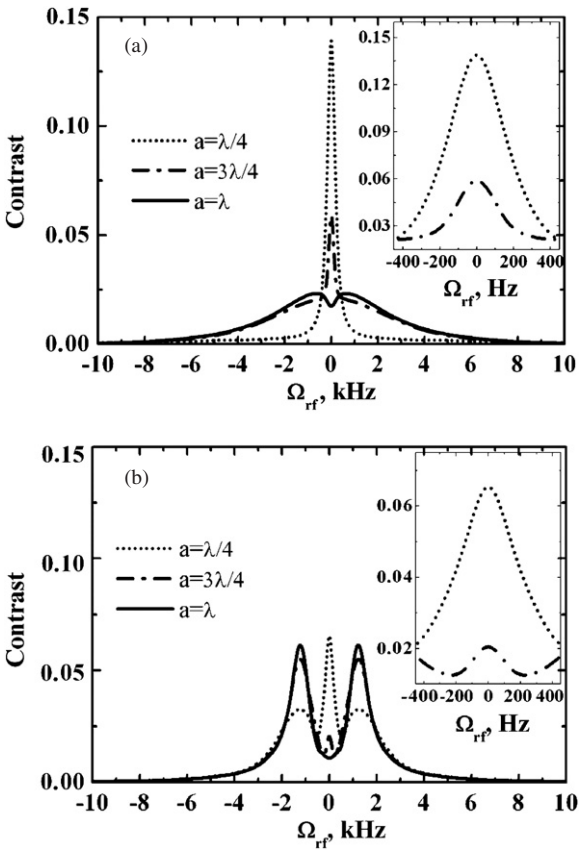

Figure 4. The DROR line contrast (dimensionless) versus the microwave field detuning for different ratios of the cell length a to the microwave radiation wavelength λ. The cell is coated, and the specular-coherent boundary conditions (15) are assumed. The ground-state coherence relaxation rate $\Gamma_\perp = 100\ s^{-1}$, the microwave Rabi frequency $U^0 = 300\ s^{-1}$, the laser intensity $I = 20\ \mu W\ cm^{-2}$: (a) 'broad-band' laser and (b) 'narrow-band' laser.

second-order Zeeman shift is present for it. In our calculations we assume that $\mathbf{B} = 0.05$ G.

We study the shape of the DROR signal for the two types of laser, differing by the laser spectrum width. For the sake of brevity, we call the laser with the spectrum width $\Gamma_L \approx \Delta_D$ a 'broad-band' laser and the laser with $\Gamma_L \leqslant \gamma$ a 'narrow-band' laser.

3.1. The specular-coherent boundary conditions

In figure 4, we present the results of our numerical calculations for the boundary conditions (15). We first consider the case of a 'broad-band' laser (figure 4(a)). The plotted curves differ in ratio a/λ, with a being the cell length and λ being the wavelength of the microwave radiation. The influence of the Dicke narrowing [24] on the DROR resonance shape for $a < \lambda$ is apparent in the cases of $a = \lambda/4$ and $a = 3\lambda/4$. If the cell length exceeds the wavelength of the microwave radiation, then the effect of the radio-induced transport (RIT) of the pure or mixed quantum states (first considered in [15, 25, 26] for the three-level model) strongly influences the DROR shape.

The physical essence of the RIT effect is the one caused by the Doppler effect velocity selectivity of the interaction

of radio (or microwave) field with active atoms, resulting in Bennett dips and peaks [27] in the velocity distribution of atoms in the ground-state sublevels coupled to the microwave radiation. Asymmetry of the two velocity distributions gives rise to the opposite-directed (along the microwave propagation direction) fluxes of the atoms in these two states. Therefore, a flux of the population inversion (or, equivalently, of the longitudinal magnetization) arises, leading to spatial separation of atoms in the two ground-state sublevels, coupled to the microwave field (for details, see [26]).

Then consider the pumping by a 'narrow-band' laser (figure 4(b)). The influence of the Dicke narrowing to the DROR shape for $a \leqslant \lambda$ is still observed. However, the DROR contrast drops by a factor of 2, compared to the case of the 'broad-band' laser excitation, since only atoms belonging to the resonant velocity group contribute to the signal formation in the case of a 'narrow-band' laser. The next important feature of the 'narrow-band' laser regime is the influence of the laser-induced transport (LIT) [28, 29] of quantum states to the DROR shape, observed for $a \geqslant \lambda/8$. It is noteworthy that the simplified three-level model of the DROR formation does not exhibit the LIT effect [15].

The LIT effect is quite similar to the RIT, namely, two counter-propagating fluxes of atoms in different states appear. However, in the LIT case, the emergence of Bennett dips and peaks and, subsequently, the asymmetry of the velocity distribution of atoms in different states, is caused by 'narrow-band' coherent radiation and is more robust to variations of the microwave field parameters. In particular, the LIT effect is present in a standing microwave field as well as in a running one, in contrast to the RIT, which takes place only in the running microwave field configuration.

Although the RIT or LIT effects may be quite important for the DROR line shape formation in a certain case, there are also many factors that suppress the RIT and LIT influence. First of all, in small cells ($a < \lambda/8$) these effects become negligible. Secondly, the one-dimensional model of an infinite-slab cell adopted in the present work tends to overestimate these effects. In real cells, with the diameter smaller than or of the order of their length in the light propagation direction, the presence of the walls in all three directions reduces the RIT and LIT effects significantly, and so does the frequency modulation of the microwave field. In our opinion, clear and unambiguous detection of the RIT and LIT effects is a hard experimental task: thermal motion of atoms in the radial dimensions and weakness of the applied microwave and optical fields precluded the LIT influence to the DROR shape in most of the experiments [1, 14, 30]. The LIT effects have been detected for the DROR with strong exciting fields [31] in a glass cell without an anti-relaxant covering (we consider such a case in the next subsection).

In contrast, the results concerning the Dicke narrowing still hold true, if we take into account the thermal motion of atoms in three dimensions [32]. We briefly recall the main results of [32]. In the one-dimensional model the atomic mean free path is equal to the cell length a, and the frequency of the wall collisions is $\nu = |v_z|/a$, with v_z being the atomic velocity. This is equivalent to the frequency modulation of the microwave radiation at the frequency ν that results in emergence (additionally to the central frequency ν_{21}) of two sidebands at $\nu_{21} \pm \nu$. Therefore, averaging of the Maxwellian distribution of v_z brings about not only a sharp central peak but also a broad 'pedestal'. In a real situation of a three-dimensional cell, the atomic mean free path has values in the interval from zero to a (or the cell diameter, if it is less than a). This makes the modulation frequency ν continuous, and the sidebands become broad. The shape of the 'pedestal' changes, but the sharp central peak persists, thus signifying the Dicke narrowing. It is noteworthy that the effects of three-dimensional geometry make the Dicke narrowing more apparent, although they hinder the LIT and RIT.

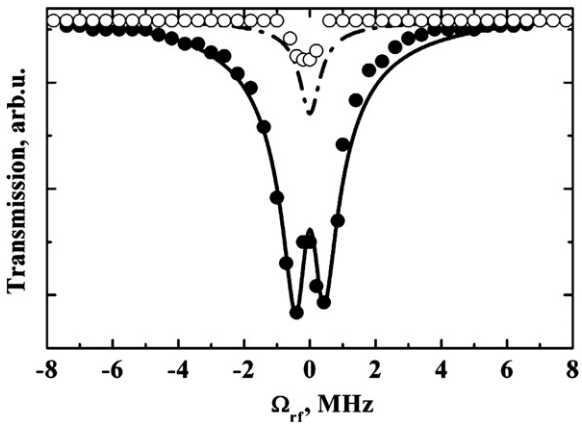

Figure 5. The DROR line versus microwave field detuning. The cell is uncoated, the complete quenching boundary conditions (16) are assumed. The pumping laser is 'narrow-band'. Points: experimental data [31]. Lines: our numerical results. DROR parameters are taken from [31].

The main difference between the DROR contrast predictions by our model that takes into account the whole hyperfine and Zeeman structure of the involved ^{87}Rb states and the simplified three-level model [15] stems from the presence of 'pocket' states, which are not taken into account in the three-level model. However, atoms can be accumulated in the 'pocket' states, decreasing the DROR contrast by a factor of 5 or even more. Therefore, we conclude that adequate description of the DROR resonance amplitude requires accounting for the whole real structure of the atomic levels. However, the three-level model is sufficient to correctly predict the DROR resonance width.

3.2. The complete quenching boundary conditions

The DROR signal in an uncoated glass cell is too low to be detected for relative small powers of laser and microwave fields. The laser power and the microwave Rabi frequency should be increased by several orders of magnitude to provide a detectable DROR signal in this case. A complicated structure of the DROR signal was detected in an experiment [31] on the strong-field excitation of ^{85}Rb vapour. We compared our numerical results with the experimental data [31] and found a good agreement (figure 5), thus proving the LIT influence to the DROR signal shape.

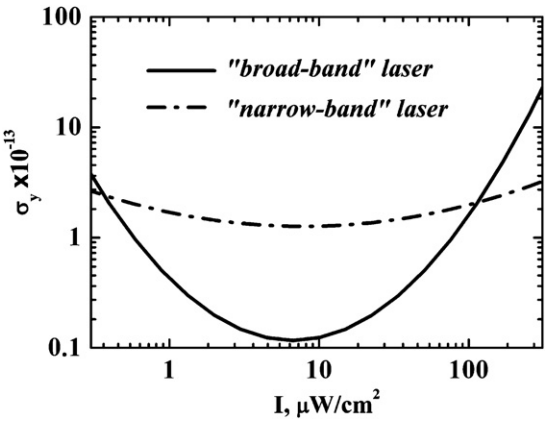

Figure 6. Short-term stability (for $\tau = 1$ s) versus laser intensity for a coated cell (boundary conditions (15)). The system parameters: $a = 3$ cm ($\lambda = 4$, 4 cm for ^{87}Rb), $\Gamma_\perp = 100\ \mathrm{s}^{-1}$.

4. Short-term stability in the shot-noise limit

Here we analyse the short-term stability $\sigma_y(\tau)$ of a quantum frequency standard with the active atoms being contained in a cell with an anti-relaxation coating. The short-term stability (Allen deviation) is inversely proportional to the figure of merit and is given in the shot-noise limit by the following expression [5, 19]:

$$\sigma_y(\tau) = \frac{\sqrt{j \cdot \mathrm{e}}}{S \cdot \Gamma_S \cdot \omega_{\mathrm{hfs}} \sqrt{\tau}}. \qquad (19)$$

Here e is the electron charge, ω_{hfs} is the working (hyperfine) transition frequency, τ is the integration time, Γ_S is the width of the linear part of the discrimination curve, i.e. the frequency range near the resonance, where the second derivative of the photodetector current j over the detuning Ω_{rf} is practically constant. The absolute value of this second derivative near the resonance (the steepness) is denoted by S.

In figure 6, we show the dependence of σ_y on the laser field intensity. The best short-term stability (1×10^{-14} for $\tau = 1$ s) is attained for a 'broad-band' laser and is by an order of magnitude worse in the case of a 'narrow-band' laser. The optimum laser intensity lies within the range from 6 μW cm^{-2} to 10 μW cm^{-2}. The reason for the better performance of the standard using a 'broad-band' laser is the greater fraction of atoms contributing to the DROR signal formation. Pumping by a 'narrow-band' laser can yield $\sigma_y \sim 10^{-13}$ for $\tau = 1$ s. Our theoretical estimations are corroborated by the experiment [33] where the short stability is of about 2×10^{-13} for $\tau = 1$ s. Note that our estimations are obtained in the idealized limit of the shot noise, i.e. without taking into account the amplitude noise and slow phase drift of the laser, noise of the electronic equipment, etc.

5. Conclusions

We studied the formation of the double radio-optical resonance in ^{87}Rb vapour in a cell with an anti-relaxation coating. The two regimes of excitation are examined, depending on a broad ($\Gamma_L \approx \Delta_D$) or narrow ($\Gamma_L \leqslant \gamma$) width of the spectrum of the laser. We show, by comparing to our numerical analysis that takes into account the whole hyperfine and Zeeman structure of the involved ^{87}Rb states, that the three-level model [15] correctly describes the Dicke narrowing of the DROR line. The 'narrow-band' laser excitation regime allows for observation of the laser-induced transport of the long-lived atomic states via its influence to the DROR signal shape. This effect was not detected in [15] where the DROR was excited by a gas discharge lamp.

The use of the 'broad-band' laser allows for improving the short-term stability of a DROR-based quantum frequency standard by an order of magnitude, compared to the case of a 'narrow-band' laser, and attaining the Allen deviation $\sigma_y = 1 \times 10^{-14}$ for the integration time $\tau = 1$ s. Although we mainly considered the applications to quantum frequency standards, our results can find an application in the development of high-precision quantum magnetometers.

Acknowledgments

This work is supported by INTAS-CNES-NSAU (project 06-1000024-9321) and the Fund of Non-Profit Programs 'Dynasty'.

References

[1] Budker D *et al* 2005 *Phys. Rev.* A **71** 012903
[2] Balabas M V *et al* 2006 *J. Opt. Soc. Am.* B **23** 1001
[3] Hodby E, Donley E A and Kitching J 2007 *Appl. Phys. Lett.* **91** 011109
[4] Knappe S *et al* 2006 *J. Opt. A: Pure Appl. Opt.* **8** S318
[5] Vanier J and Audoin C 1989 *The Quantum Physics of Atomic Frequency Standards* (Bristol: Hilger) p 1567c
[6] Huss A *et al* 2006 *J. Opt. Soc. Am.* B **23** 1729
[7] Shah V *et al* 2007 *Nat. Photon.* **1** 649
[8] Budker D and Romalis M 2007 *Nat. Phys.* **3** 227
[9] Acuna M H 1997 *Encyclopedia of Planetary Sciences* ed J H Shirley and R W Fairbridge (London: Chapman and Hall) p 406
[10] Lukin M D *et al* 1999 *Phys. Rev.* A **60** 3225
[11] Yelin S F *et al* 2003 *Phys. Rev.* A **68** 063801
[12] Robinson H, Ensberg E and Dehmelt H T 1958 *Bull. Am. Phys. Soc.* **3** 9
[13] Graf M T *et al* 2005 *Phys. Rev.* A **72** 023401
[14] Guzman J S *et al* 2006 *Phys. Rev.* A **74** 053415
[15] Agap'ev B D, Gornyi M B and Matisov B G 1988 *Sov. Phys.—Tech. Phys.* **33** 1394
[16] Varshalovich D A, Moskalev A N and Khersonskii V K 1988 *Quantum Theory of Angular Momentum* (Singapore: World Scientific)
[17] Kazakov G A *et al* 2006 *Tech. Phys.* **51** 1414
[18] Matisov B G and Mazets I E 1992 *Opt. Commun.* **92** 247
[19] Gornyi M B *et al* 1987 *Sov. Phys.—Tech. Phys.* **32** 448
[20] Agap'ev B D, Gornyi M B, Matisov B G and Rozhdestvenskii Yu V 1993 *Phys.—Usp.* **36** 763
Arimondo E 1996 *Progress in Optics* vol XXXV, ed E Wolf (North-Holland: Elsevier) p 257
[21] Deng J 2001 *IEEE* **48** 1657
[22] Kazakov G *et al* 2006 *Proc. EFTF-2006—WeP12*
[23] Kazakov G *et al* 2005 *Phys. Rev.* A **72** 063408
[24] Dicke R H 1953 *Phys. Rev.* **89** 472
[25] Agap'ev B D and Matisov B G 1986 *Sov. Tech. Phys. Lett.* **12** 51

[26] Agap'ev B D and Matisov B G 1986 *JETP Lett.* **44** 81
[27] Bennett W R 1962 *Phys. Rev.* **126** 580
[28] Agap'ev B D, Gornyi M B and Matisov B G 1986 *Opt. Spektr.* **61** 1155
[29] Agap'ev B D, Gornyi M B and Matisov B G 1987 *Sov. Phys.—JETP* **65** 1121
[30] Klein M *et al* 2006 *J. Mod. Opt.* **53** 2583
[31] Zibrov A S *et al* 2006 *JETP Lett.* **83** 168
[32] Frueholz R P and Volk C H 1985 *J. Phys. B: At. Mol. Phys.* **18** 4055
[33] Szekely C *et al* 1993 *Proc. IEEE Int. Frequency Control Symp.* pp 41518–21